

# Modeling of a Complementary and Modular Linear Flux-Switching Permanent Magnet Motor for Urban Rail Transit Applications

Ruiwu Cao, *Student Member, IEEE*, Ming Cheng, *Senior Member, IEEE*, Chris Mi, *Fellow, IEEE*, Wei Hua, *Member, IEEE*, Xin Wang, and Wenxiang Zhao, *Member, IEEE*

**Abstract**—In this paper, a complementary and modular linear flux-switching permanent magnet (MLFSPM) motor is investigated, in which both the magnets and armature windings are placed in the short mover, while the long stator consists of iron core only. The proposed MLFSPM motor incorporates the high power density of a linear permanent magnet synchronous motor and the simple structure of a linear induction motor. It is especially suitable for long stator applications such as urban rail transit. The objective of this paper is to build the mathematical model for the purpose of control of this motor. The simulation results by means of finite-element analysis (FEA) verified the theoretical analysis and the effectiveness of this model. Both the analytical model and the FEA results are validated by experiments based on a prototype motor.

**Index Terms**—Flux-switching permanent magnet (FSPM) motor, linear motor, modeling.

## I. INTRODUCTION

FOR urban rail transit (URT), a direct drive linear motor has the benefits of faster dynamic performance, improved reliability, lower noise, lower cost of road maintenance, and lower pollution due to the elimination of unnecessary energy conversion from rotary to linear motion when compared to rotary machines [1]–[5]. Also, when used in subways, it can reduce the tunnel radius to save construction cost [6]. The conventional permanent magnet (PM) linear motor exhibits higher efficiency and higher power factor than induction linear motor [7]. However,

in long stator applications such as URT, this solution inevitably results in significant cost increase due to a large amount of magnets or armature windings set on the long stator. In recent years, a new class of PM brushless motors with magnets and armature winding all located in the stator, namely the flux-switching permanent magnet (FSPM) and doubly salient permanent magnet (DSPM) motors [8]–[11], have received wide attentions due to its high power density, fault-tolerant property [12]–[14], robust mechanical integrity, and free from thermal stress problem. Recently, the linear structure of FSPM motors [15]–[17] and DSPM motor [18] have attracted much attention, in which both the PMs and armature windings are all located in the short mover, while the long stator only consists of iron core. Hence, these linear FSPM (LFSPM) and linear DSPM (LDSPM) motors are suitable for long stator applications. Furthermore, in order to solve the drawbacks such as asymmetrical magnetic circuit, large cogging force in the existing LFSPM and LDSPM motor, modular, and complementary linear FSPM (MLFSPM) and DSPM (MLDSPM) motors have been proposed and investigated in [19] and [20], respectively. Due to its complementary structure, the phase flux-linkage and back-EMF waveform are symmetrical, the three-phase flux linkage and back-EMF are balanced, and the total cogging force is smaller.

For URT application, direct force control, or voltage space vector control are often needed to control the motor. For this purpose, a mathematical model of the MLFSPM motor based on synchronous  $d$ - $q$  frame is necessary.

Hence, the objective of this paper is to build the mathematical model of this MLFSPM motor that can be used for the control development of the proposed MLFSPM motor. In Section II, the topology and principle of the proposed MLFSPM motor will be introduced. In Section III, the steady-state characteristics including flux linkage, EMF, inductance, and cogging force are analyzed using finite-element analysis (FEA) that serves as the basis of the mathematical models. In Section IV, the mathematical models based on stator frame and  $d$ - and  $q$ -frames are developed. To verify the model of the MLFSPM motor, a prototype motor has been built and tested, and the results are discussed in Section V. Finally, some conclusions are drawn in Section VI.

## II. TOPOLOGY AND PRINCIPLE

### A. Topology

Fig. 1(a) shows the topology of the modular linear flux-switching PM motor. Each phase consists of two “E”-shaped

Manuscript received October 5, 2011; revised January 28, 2012; accepted March 6, 2012. Date of publication April 9, 2012; date of current version May 18, 2012. This work was supported by the National Natural Science Foundation of China under Project 50907031, by the Specialized Research Fund for the Doctoral Program of Higher Education of China under Project 20090092110034, and by the Program for Postgraduate Research Innovation in the University of Jiangsu Province 2010 under Project X10B\_066Z. Paper no. TEC-00516-2011.

R. Cao is with the School of Electrical Engineering, Southeast University, Nanjing 210096, China and also with the Department of Electrical and Computer Engineering, University of Michigan, Dearborn, MI 48128 USA (e-mail: ruiwucao@gmail.com).

M. Cheng, X. Wang, and W. Hua are with the School of Electrical Engineering, Southeast University, Nanjing 210096, China (e-mail: mcheng@seu.edu.cn; 18724015102@163.com; huawei1978@seu.edu.cn).

C. Mi is with the Department of Electrical and Computer Engineering and the DOE GATE Center for Electric Drive Transportation, University of Michigan, Dearborn, MI 48128 USA (e-mail: mi3032@gmail.com).

W. Zhao is with the School of Electrical and Information Engineering, Jiangsu University, Zhenjiang 212013, China (e-mail: zwx@ujs.edu.cn).

Color versions of one or more of the figures in this paper are available online at <http://ieeexplore.ieee.org>.

Digital Object Identifier 10.1109/TEC.2012.2190985

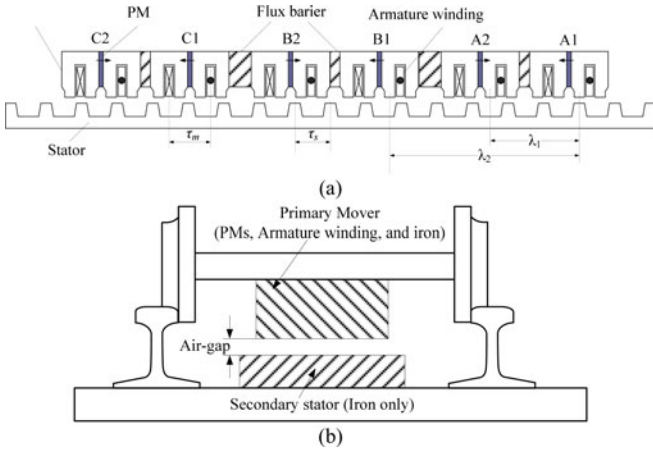


Fig. 1. Schematic diagram of the MLFSPM motor and linear motor vehicle. (a) MLFSPM motor. (b) Linear motor vehicle.

modules whose positions are mutually  $\lambda_1$  apart:

$$\lambda_1 = \left(k + \frac{1}{2}\right) \tau_s \quad (1)$$

where  $\tau_s$  is the stator pole pitch,  $k$  is a positive integer ( $k = 2$ ). Each “E”-shaped module consists of two “U”-shaped iron, between which a PM is sandwiched. The armature winding coils are located in the slot and wound around the adjacent teeth of the two “U” modules. The two coils of phase A, namely coil A1 and coil A2, are connected in series. The two PMs in the two “E” modules are magnetized in opposite directions. The structure of phase B and phase C is the same as that of phase A.

For a three-phase motor, the relative displacement between the module of the adjacent two phases is equal to  $\lambda_2 = (j + 1/m)\tau_s$ , where  $j$  is a positive integer ( $j = 5$ ),  $m$  is the number of phases ( $m = 3$ ). There is a flux barrier between every two adjacent “E” modules. The principle of the MLFDPM motor used for railway application is shown in Fig. 1(b), in which the short primary mover consisting of PM, armature winding, and iron is fixed under the bogie of a railway vehicle and the secondary long stator is fastened between the two iron rails.

### B. Operation Principle

Fig. 2 shows the open circuit field distribution of the proposed linear motor at different mover positions obtained by FEA. At the initial position as shown in Fig. 2(a), the “E” module of coil A1 (“E1”) is in symmetry with the “E” module of coil A2 (“E2”) along the central axis of stator slot. Assuming that the flux linkage induced in coils A1 and A2 reaches the negative maximum value at the initial position, when the mover moves to the position as shown in Fig. 2(b), the flux linkage induced in coils A1 and A2 is nearly equal to zero. Because the magnet circuits in “E1” and “E2” are different, the position of module “E1” can be defined as “first balance position” and the position of module “E2” can be noted as “second balance position.” At position  $\theta_e = 180^\circ$  as shown in Fig. 2(c), “E1” is in symmetry with “E2” along the central axis of stator teeth, where the flux linkage induced in coils A1 and A2 reaches the positive maxi-

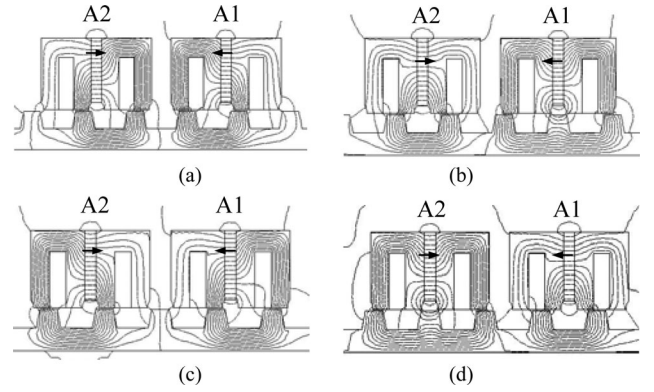


Fig. 2. Open circuit field distributions of the proposed motor at four mover positions (a)  $\theta_e = 0^\circ$ . (b)  $\theta_e = 90^\circ$ . (c)  $\theta_e = 180^\circ$ . (d)  $\theta_e = 270^\circ$ .

imum value. Also, at position  $\theta_e = 270^\circ$  as shown in Fig. 2(d), “E1” moves to the “second balance position” and “E2” to the “first balance position.” So, when the mover moves by one stator pole pitch, the flux linkage of coil A1 and coil A2 is bipolar, complementary and symmetrical.

### III. STEADY-STATE CHARACTERISTICS OF THE MLFSPM MOTOR

In this section, the steady-state characteristics of the proposed motor, including the PM flux-linkage, back-EMF, self- and mutual inductance, and its harmonics are analyzed and investigated using FEA. Fig. 3(a) shows the PM flux-linkage waveform in phase A. It should be noted that it contains a small dc component. The frequency spectrum of the PM flux linkage is illustrated in Fig. 3(b). It can be seen that it is nearly sinusoidal, and the total harmonics distortion (THD) is only 1.13%. Fig. 4 depicts the corresponding back-EMF waveforms induced in phase A at the rated speed and its harmonics. It can be found that the even harmonics in the phase back-EMF are significantly reduced. Hence, the back-EMF is also sinusoidal and its THD is only 1.52%.

The self-inductance and its harmonics are shown in Fig. 5. Obviously, the second, third and fourth harmonics in the inductance are significant and the THD is about 23%. The mutual inductance waveform is shown in Fig. 6. It can be seen that the mutual inductance of the proposed motor is very small. The key information of the flux-linkage, back-EMF, and inductance is listed in Table I. It can be seen from Table I that the dc components  $\psi_0$  of the flux linkage is about 10% of the peak value of the fundamental component of the flux linkage. Also, the peak value of the fundamental component of self-inductance  $L_m$  is about 2.6% of its dc component. Hence, the harmonic components of the inductance can be neglected. Moreover, the dc components of mutual inductance  $L_{ab}$  and  $L_{bc}$  as shown in Fig. 6 are only about 3.15% of the self-inductance  $L_{DC}$ , and  $L_{ca}$  is nearly zero. So, the mutual inductance of the MLFSPM motor can be neglected.

Fig. 7 shows the cogging force of the MLFSPM motor, in which “Cogging\_A” denotes the cogging force waveform of the two “E” module of phase A based on FEA. “Cogging\_B” and “Cogging\_C” denote the cogging force waveforms of the

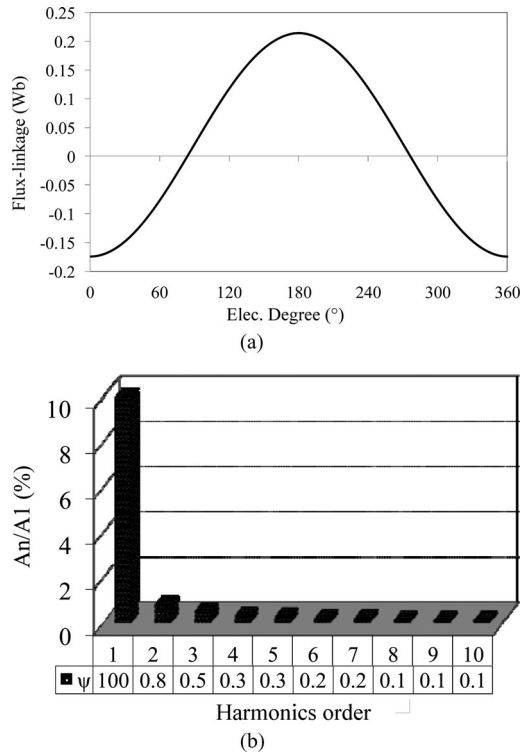


Fig. 3. Flux linkage and its harmonics. (a) Flux linkage. (b) Harmonics distribution.

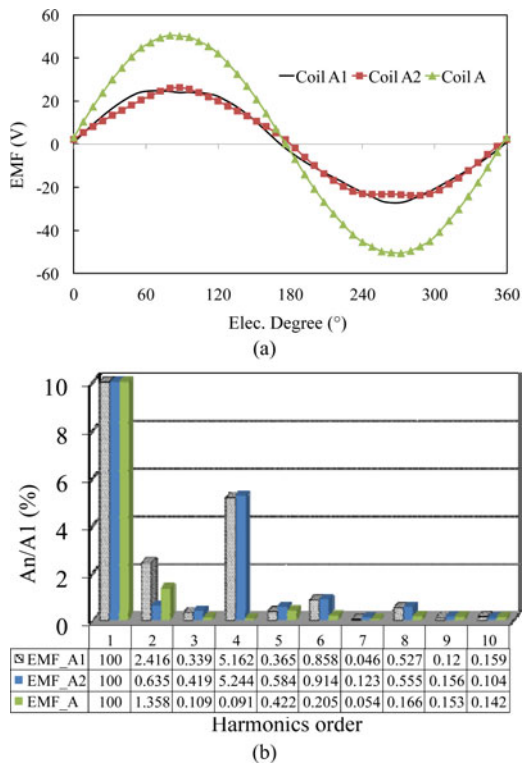


Fig. 4. Back-EMF and its harmonics. (a) EMF. (b) Harmonics distribution.

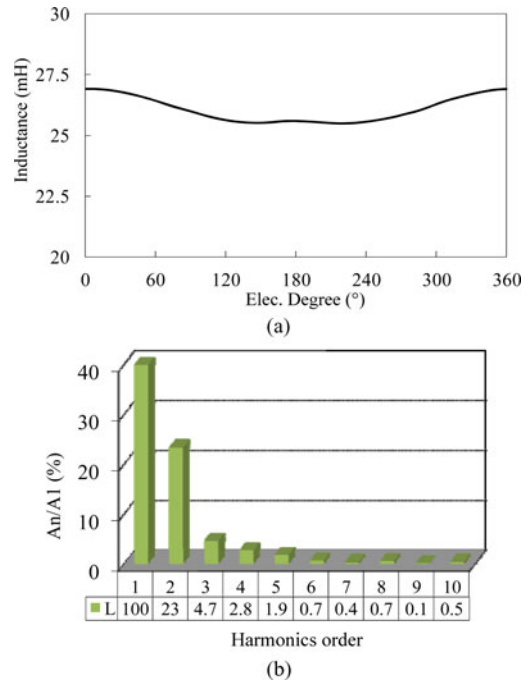


Fig. 5. Self-inductance and its harmonics. (a) Self-inductance. (b) Harmonics distribution.

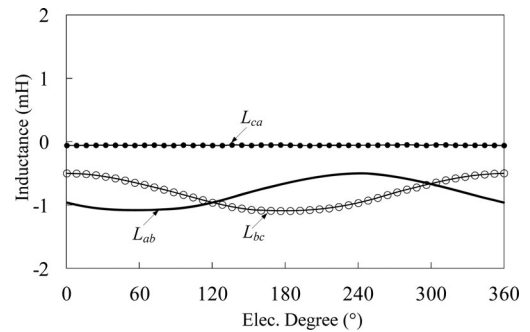


Fig. 6. Mutual inductance.

TABLE I  
CHARACTERISTICS OF FLUX LINKAGE, EMF, AND INDUCTANCE

Items	Flux Linkage (Wb)	EMF (V)	Inductance (mH)
DC component	0.01994	0	26.07
Fundamental (Peak)	0.1943	50.64	0.6787
THD (%)	1.126	1.5	24.2

modules of phase B and phase C, which are obtained by shifting “Cogging\_A” by 120° and 240° electrical degrees, respectively. Also, “Cogging\_sum” is the sum of “Cogging\_A,” “Cogging\_B,” and “Cogging\_C.” “Cogging\_whole” is the total cogging force of the LFSPM motor calculated directly by means of FEA. It should be noted that there are some errors between the total cogging force based on the two methods, which we believe is caused by the omission of the end effect in the first method. However, it can illustrate that the total cogging force is weakened by the three-phase complementary and modular structure.

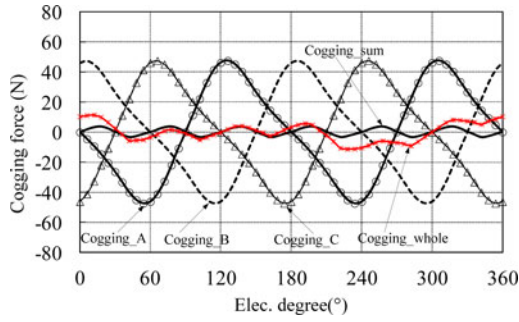
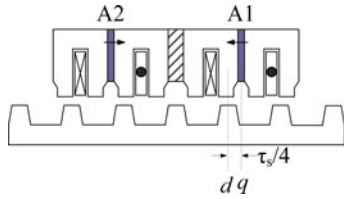


Fig. 7. Cogging force of the MLFSPM motor.

Fig. 8. Definition of  $d$ - and  $q$ -axes.

#### IV. MATHEMATIC MODEL OF THE MLFSPM MOTOR

##### A. Mathematic Model in Stator Reference Frame

From Fig. 3, the three-phase PM flux linkage of the proposed MLFSPM motor can be expressed as

$$\begin{cases} \psi_{ma} = \psi_0 - \psi_m \cos(\theta_e) \\ \psi_{mb} = \psi_0 - \psi_m \cos(\theta_e - 120^\circ) \\ \psi_{mc} = \psi_0 - \psi_m \cos(\theta_e + 120^\circ) \end{cases} \quad (2)$$

where  $\psi_0$  is the dc component,  $\psi_m$  is the peak value of the fundamental component as shown in Table I, and  $\theta_e$  is the electrical degree of the mover position.

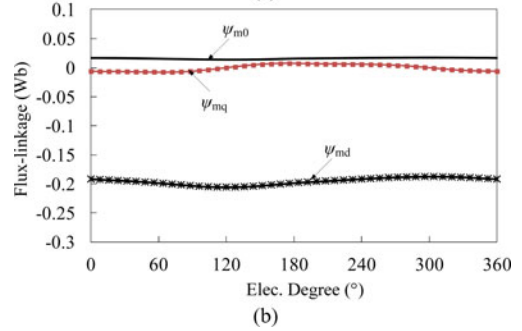
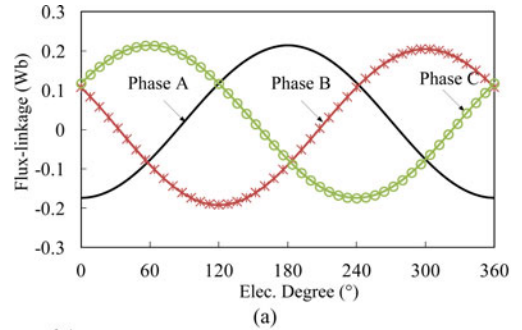
It can be seen from Figs. 5 and 6, and Table I that the mutual inductance  $L_{ab}$ ,  $L_{bc}$ , and  $L_{ca}$  can be neglected and the three-phase self-inductance,  $L_{aa}$ ,  $L_{bb}$ ,  $L_{cc}$  can be expressed as

$$\begin{cases} L_{aa} = L_{DC} + L_m \cos(\theta_e) \\ L_{bb} = L_{DC} + L_m \cos(\theta_e - 120^\circ) \\ L_{cc} = L_{DC} + L_m \cos(\theta_e + 120^\circ) \\ L_{ab} = L_{bc} = L_{ca} \approx 0 \end{cases} \quad (3)$$

where,  $L_{DC}$  and  $L_m$  are the dc component and peak value of the fundamental component of self-inductance respectively, as shown in Table I.

##### B. $d$ - $q$ Axis of the Proposed MLFSPM Motor

To realize the transformation from stator reference frame to mover reference frame, the  $d$ - and  $q$ -axes of the proposed MLFSPM motor is defined in Fig. 8, in which the  $d$ -axis is chosen to be the mover position where the PM flux linkage reaches the maximum value, and the  $q$ -axis is chosen to be the mover position where the value of the PM flux linkage is zero. The relative displacement between the  $d$ -axis and the  $q$ -axis is  $\tau_s/4$ .

Fig. 9. PM flux linkage in different reference frame. (a) Stator reference frame. (b)  $d$ - $q$  reference frame.

##### C. $abc$ - $dq$ Transformation

The vector control strategy is based on the synchronous mover frame that moves at synchronous speed. To get the two-phase  $d$ - $q$  axis electromagnetic parameters, the traditional Park matrix as shown in (4) is used in this paper

$$P = \frac{2}{3} \begin{bmatrix} \cos(\theta_e) & \cos(\theta_e - 120^\circ) & \cos(\theta_e + 120^\circ) \\ -\sin(\theta_e) & -\sin(\theta_e - 120^\circ) & -\sin(\theta_e + 120^\circ) \\ 1/2 & 1/2 & 1/2 \end{bmatrix}. \quad (4)$$

The matrix form of PM flux linkage in the  $d$ - $q$  frame can be derived as

$$\begin{bmatrix} \psi_{md} \\ \psi_{mq} \\ \psi_{m0} \end{bmatrix} = P \begin{bmatrix} \psi_{ma} \\ \psi_{mb} \\ \psi_{mc} \end{bmatrix} = \begin{bmatrix} -\psi_m \\ 0 \\ \psi_0 \end{bmatrix}. \quad (5)$$

It can be seen from (5) that the PM flux linkage in  $d$ -axis  $\psi_{md}$  is equal to the negative peak value of the fundamental component shown in Table I. The PM flux linkage in  $q$ -axis  $\psi_{mq}$  is equal to zero, and the PM flux linkage in  $\theta$ -axis  $\psi_{m0}$  is equal to the dc component shown in Table I. To verify the aforementioned analysis, the waveforms of the three-phase PM flux linkage versus mover position in the stator frame is calculated using FEA and the PM flux linkage in the  $d$ - $q$  reference frame is transformed from the FEA results of three-phase flux linkage as shown in Fig. 9. The average value of  $\psi_{md}$ ,  $\psi_{mq}$ , and  $\psi_{m0}$  are summarized in Table II. It can be seen that the results from math model are consistent with the FEA results.

TABLE II  
PM FLUX LINKAGE IN  $d$ - $q$  REFERENCE FRAME

Flux terms	Flux Linkage (Wb)	
	from FEA	from Math Model
$\psi_{md}$	-0.1955	-0.1943
$\psi_{mq}$	0.00011	0
$\psi_{m0}$	0.01658	0.01994

As aforementioned, by neglecting the mutual inductance, the inductances in  $d$ - and  $q$ -axis frame can be described as follows:

$$\begin{bmatrix} L_d & L_{dq} & L_{d0} \\ L_{qd} & L_q & L_{q0} \\ L_{0d} & L_{0q} & L_0 \end{bmatrix} = P \begin{bmatrix} L_{aa} & 0 & 0 \\ 0 & L_{bb} & 0 \\ 0 & 0 & L_{cc} \end{bmatrix} P^{-1} \quad (6)$$

where  $L_d$ ,  $L_q$ ,  $L_0$ ,  $L_{dq}$ ,  $L_{qd}$ ,  $L_{d0}$ ,  $L_{0d}$ ,  $L_{q0}$ , and  $L_{0q}$  are the synchronous inductance components in  $d$ - and  $q$ -axis frame. Thus, by substituting (3) and (4) into (6), the synchronous inductance components in  $d$ - and  $q$ -axis frame can be derived as

$$L_d = L_{DC} + \frac{L_m \cos(3\theta_e)}{2} \quad (7)$$

$$L_q = L_{DC} - \frac{L_m \cos(3\theta_e)}{2} \quad (8)$$

$$L_{dq} = L_{qd} = \frac{-L_m \sin(3\theta_e)}{2} \quad (9)$$

$$L_{q0} = L_{0q} = 0 \quad (10)$$

$$L_0 = \frac{(L_{aa} + L_{bb} + L_{cc})}{3} = L_{DC} \quad (11)$$

$$L_{d0} = 2 \times L_{0d} = L_m. \quad (12)$$

It can be observed from (7) to (8) that the  $d$ - and  $q$ -axis inductance,  $L_d$  and  $L_q$  are not constant, which all contain a small cosine component with three times variation frequency of that of the PM flux linkage. Generally, the mutual inductance between the  $d$ - and  $q$ -axis windings is zero, because the flux induced by a current in one winding will not link with another winding displaced in space by  $90^\circ$ . However, in the PM motor with saliency stator and rotor teeth, a part of the  $d$ -axis winding flux will link with the  $q$ -axis winding as the uneven reluctance provides a path for flux through the  $q$ -axis winding [21]. Hence, the  $d$ - and  $q$ -axis mutual inductance  $L_{dq}$  is not zero, which is a small sinusoidal waveform and equals  $L_{qd}$ .

To verify the aforementioned equations, the three-phase inductances of the MLSFPM motor are first calculated using FEA as shown in Fig. 10(a). The self-inductance components in  $d$ - and  $q$ -axes,  $L'_d$ ,  $L'_q$ , and  $L'_0$  are transformed directly from the three-phase inductance in the stator frame shown in Fig. 10(a). The average values are  $L_d = 26.085$  mH,  $L_q = 26.055$  mH,  $L'_d = 26.255$  mH, and  $L'_q = 26.085$  mH, as shown in Fig. 10(b).

On the other hand, by substituting the dc component of the inductance  $L_{DC}$  and the peak value of the fundamental inductance  $L_m$  listed in Table I into (7), (8), and (11),  $L_d$ ,  $L_q$ , and  $L_0$  can be obtained and shown in Fig. 10(b). It can be seen that there are some errors between  $L_d$ ,  $L_q$ ,  $L_0$  and  $L'_d$ ,  $L'_q$ ,  $L'_0$ , but the shape and

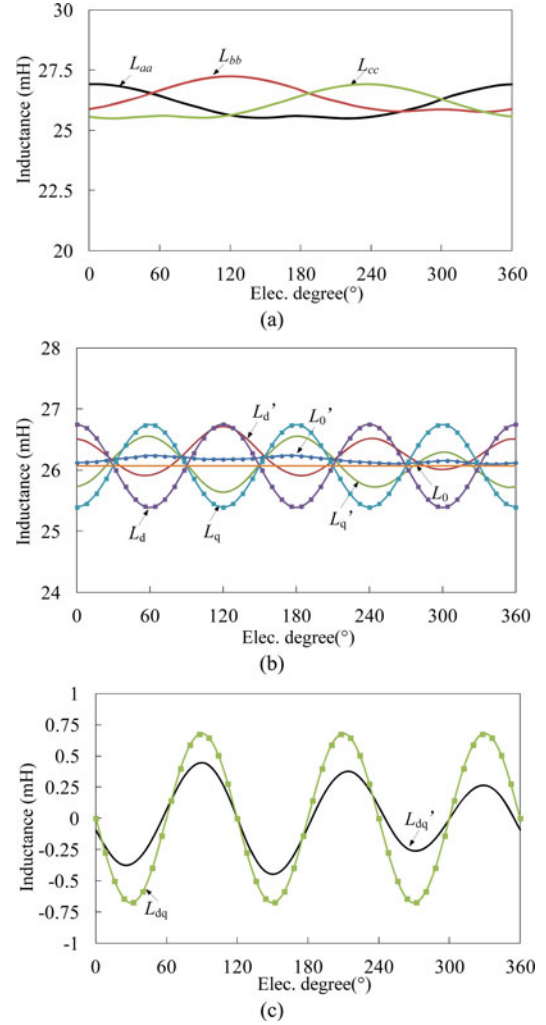


Fig. 10. Waveforms of self-inductance (a). Inductance in stator frame. (b)  $L_d$ ,  $L_q$ ,  $L_0$ , and  $L'_d$ ,  $L'_q$ ,  $L'_0$ . (c)  $L_{dq}$  and  $L'_{dq}$ .

amplitude are nearly the same. Fig. 10(c) compares the mutual inductance components in  $d$ - and  $q$ -axes,  $L_{dq}$ , and  $L'_{dq}$  by the aforementioned two methods.

In order to prove  $d$ - $q$  expression of the inductance is valid, the calculation method of  $d$ - $q$  frame inductance as discussed in [22] is adopted, namely

$$L_d = \frac{\psi_i \cos \alpha - \psi_{pm}}{I_d} \quad (13)$$

$$L_q = \frac{\psi_i \sin \alpha}{I_q} \quad (14)$$

where  $\psi_i$  is the fundamental component of the total flux linkage considering the armature reaction effects and  $\psi_{pm}$  is the fundamental component of the total flux linkage excited by PM only,  $\alpha$  is the phase difference between  $\psi_i$  and  $\psi_{pm}$ . Based on this method, the  $d$ - $q$  reference frame inductances are  $L_d = 25.89$  mH and  $L_q = 27$  mH. It can be seen that the average value of  $d$ - $q$  reference frame inductance based on mathematical method and the two FEA methods are nearly the same.

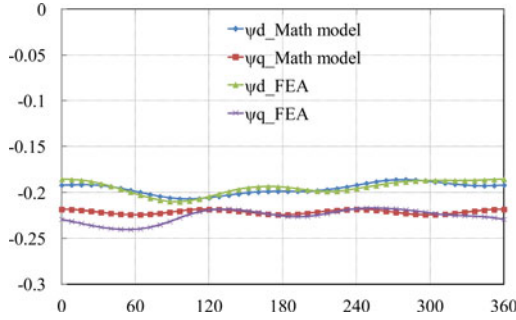


Fig. 11. Waveforms of the total flux linkage under  $i_d = 0$  control method.

#### D. Electromagnetic Force

Based on the preceding analysis, the total flux linkage in  $d$ - and  $q$ -axes can be defined as

$$\begin{cases} \psi_d = \psi_{md} + L_d i_d + L_{dq} i_q \\ \psi_q = L_q i_q + L_{dq} i_d. \end{cases} \quad (15)$$

Substituting (7), (8), and (9) into (15), it yields

$$\begin{cases} \psi_d = \psi_{md} + (L_{DC} + L_m \cos(3\theta_e)/2)i_d - i_q L_m \sin(3\theta_e)/2 \\ \psi_q = (L_{DC} - L_m \cos(3\theta_e)/2)i_q - i_d L_m \sin(3\theta_e)/2. \end{cases} \quad (16)$$

In order to prove the accuracy of (16), the total flux linkage in the  $d$ - and  $q$ -axes are calculated by two means and compared in Fig. 11, where “ $\psi_d$ -FEA” and “ $\psi_q$ -FEA” denote the total flux linkage in  $d$ - and  $q$ -axes when  $i_d = 0$  control method is adopted at the rated current, “ $\psi_d$ -Math model” and “ $\psi_q$ -Math model” denote the total flux linkage in  $d$ - and  $q$ -axes by (16). It can be seen that the shape and amplitude of the  $d$ - $q$  reference frame flux linkage based on the two methods are nearly the same.

The voltage equations in the  $d$ - and  $q$ -axes can be written as

$$\begin{cases} u_d = \frac{d\psi_d}{dt} - \omega_e \psi_q + R i_d \\ u_q = \frac{d\psi_q}{dt} + \omega_e \psi_d + R i_q. \end{cases} \quad (17)$$

Substituting (16) into (17), the voltage equations can be derived:

$$\begin{cases} u_d = -3\omega_e L_m (i_d \sin(3\theta_e) + i_q \cos(3\theta_e))/2 - \omega_e \psi_q + R i_d \\ u_q = 3\omega_e L_m (i_q \sin(3\theta_e) - i_d \cos(3\theta_e))/2 + \omega_e \psi_d + R i_q \end{cases} \quad (18)$$

where  $\omega_e = 2\pi v/\tau_s$  is the electrical angular frequency, and  $v$  is the mover speed.

From (18), the output thrust force of the three-phase MLFSPM motor can be derived as

$$\begin{aligned} F_o &= \frac{3}{2} \frac{(((d\psi_d/dt) - \omega_e \psi_q) i_d + (d\psi_q/dt + \omega_e \psi_d) i_q)}{v} \\ &= \frac{3\pi}{\tau_s} [\psi_{md} i_q + i_d i_q (L_d - L_q) + L_{dq} (i_q^2 - i_d^2)] \\ &\quad + \frac{9\pi}{2\tau_s} L_m (i_q^2 - i_d^2) \sin 3\theta_e \\ &= \frac{3\pi}{\tau_s} \psi_{md} i_q + \frac{3\pi}{\tau_s} i_d i_q (L_d - L_q) \end{aligned}$$

$$\begin{aligned} &+ \frac{3\pi}{\tau_s} L_m (i_q^2 - i_d^2) \sin 3\theta_e \\ &= F_{pm} + F_r + F_{Lm} \end{aligned} \quad (19)$$

where  $F_{pm}$  is the PM thrust force,  $F_r$  is the reluctance thrust force, and  $F_{Lm}$  is an additional force component, which is caused by the fluctuation of the self inductance  $L_m$ . If  $L_m$  is neglected, the output thrust force can be expressed as

$$F_o = \frac{3\pi}{\tau_s} [\psi_{md} i_q + i_d i_q (L_d - L_q)]. \quad (20)$$

When  $i_d = 0$  control method is adopted, namely, the three-phase currents are in phase with the back-EMF and can be expressed as

$$\begin{cases} I_a = I_m \sin(\theta_e) \\ I_b = I_m \sin(\theta_e - 120^\circ) \\ I_c = I_m \sin(\theta_e + 120^\circ) \end{cases} \quad (21)$$

where,  $I_m$  is the peak value of the phase current. Thus, the phase current in  $d$ - and  $q$ -axes can be transformed as

$$\begin{cases} I_d = 0 \\ I_q = -I_m \\ I_0 = 0. \end{cases} \quad (22)$$

By substituting (22) into (19), the output thrust force can be derived as

$$F_o = \frac{3\pi}{\tau_s} (-\psi_{md} I_m + L_m I_m^2 \sin 3\theta_e). \quad (23)$$

It can be seen from (23) that the thrust force consists of two components, namely a dc component and a sinusoidal component with three times variation frequency of that of the PM flux linkage. Hence, the thrust force ripple can be defined as

$$K_{\text{ripple}} = \frac{F_{\max} - F_{\min}}{F_{\text{avg}}} \times 100 = \frac{2L_m I_m}{-\psi_{md}} \times 100 \quad (24)$$

where  $F_{\max}$  is the maximum value of the thrust force,  $F_{\min}$  is the minimum value of thrust force, and  $F_{\text{avg}}$  is the average value of thrust force. Equation (24) depicts that the thrust force ripple is proportional to the peak value of the phase current.

By substituting  $L_m = 0.6787$  mH,  $I_m = 6 \times 1.414$  A,  $\psi_{md} = -0.1955$  Wb,  $\tau_s = 0.036$  m into (23), the output thrust force can be drawn and noted as “ $F_o$ -Math model” as shown in Fig. 12. To verify the aforementioned theoretical analysis, the thrust force of the MLFSPM motor was also calculated by FEA and noted as “ $F_o$ -FEA” as shown in Fig. 12. It should be noted that the cogging force value is not included in “ $F_o$ -FEA.” The key values of “ $F_o$ -Math model” and “ $F_o$ -FEA” are listed in Table III. Obviously, the shape, period, and average value of “ $F_o$ -Math model” and “ $F_o$ -FEA” are nearly the same. The thrust force ripple of MLFSPM motor is less than 6%.

#### V. EXPERIMENT RESULTS

To validate the mathematical model of the MLFSPM motor and associated FEA analysis, experiments are conducted on a three-phase MLFSPM motor prototype as shown in Fig. 13. The detailed design specifications are listed in Table IV. Fig. 14(a)

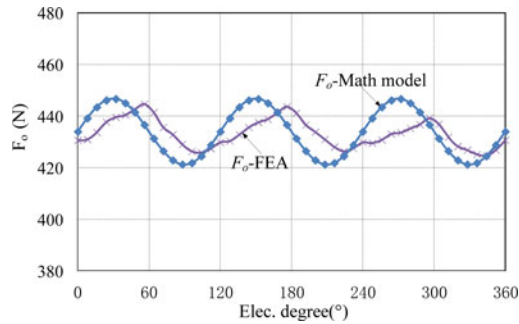


Fig. 12. Output thrust force waveforms.

TABLE III  
CHARACTERISTICS OF THRUST FORCE AND COGGING FORCE

Items	$F_o$ FEA	$F_o$ Math model
Maximum (N)	444.7	446.7
Minimum (N)	424.72	421.3
Average (N)	434.71	434
$K_{ripple}$ (%)	4.6	5.85

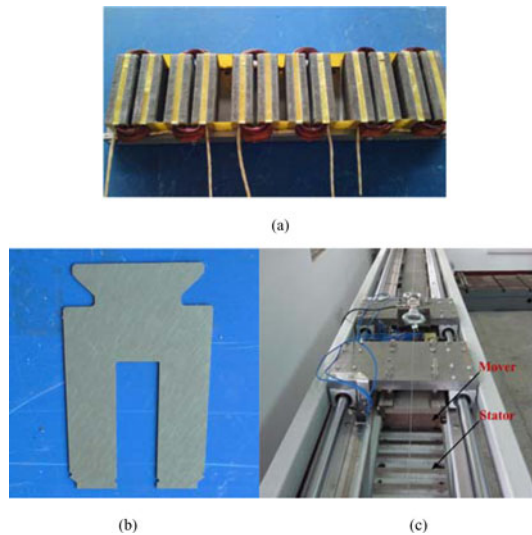


Fig. 13. Prototype of MLFSPM. (a) Mover structure and armature winding. (b) Mover "U"-shaped laminated segments. (c) Prototype motor.

illustrates the calculated self-inductances at different currents (applied 6 and 1 A) by means of FEA, from which it can be seen that the self-inductance under 6-A applied current is smaller than the one under 1-A applied current in the range from  $60^\circ$  to  $300^\circ$  electrical degree due to the higher saturation under 6-A applied current. Fig. 14(b) compares the measured self-inductance with the calculated self-inductance under 1-A applied current. Obviously, the measured inductance waveform matches well with the simulated inductance. Also, the simulation and measured open circuit back-EMF at speed of 1.392 m/s are compared in Fig. 15. It can be seen that the simulation results exhibit a good agreement with the experimental result. The discrepancies be-

TABLE IV  
DESIGN SPECIFICATIONS OF THE PROPOSED MOTOR

Rated speed, $v$ (m/s)	1.5
Mover width, $l_m$ (mm)	120
Mover tooth width, $w_{mt}$ (mm)	10.5
Mover slot width, $w_{st}$ (mm)	10.5
Mover high, $h_m$ (mm)	50
Mover yoke high, $h_{my}$ (mm)	14
Mover slot mouth width, $w_{msm}$ (mm)	10.5
Mover pole pitch, $\tau_m$ (mm)	42
Stator pole pitch, $\tau_s$ (mm)	36
Permanent magnet high, $h_{pm}$ (mm)	30
Permanent magnet width, $w_{pm}$ (mm)	7
Magnet remanence, $B_r$ (T)	1.2
Magnet relative recoil permeability, $\mu_r$	1.05
Air gap length, $g$ (mm)	2
Armature windings per coil, $N_{coil}$	116 turns
Rated Armature current, $I_{RMS}$ (A)	6

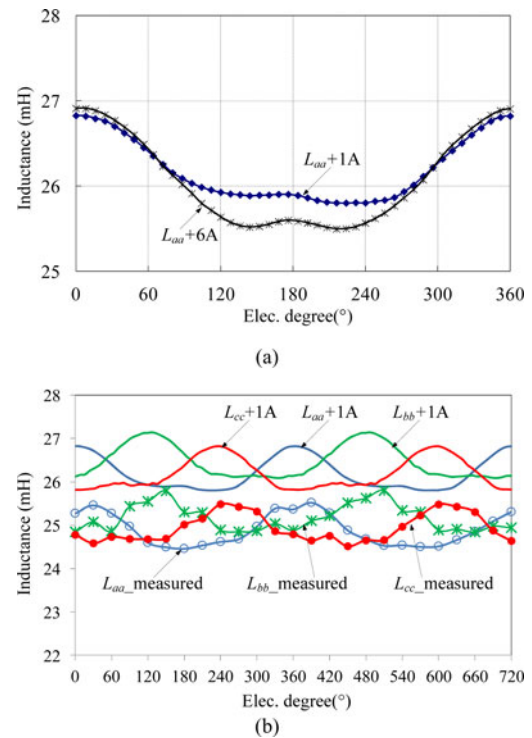


Fig. 14. Self-inductance. (a) Simulated self-inductance at different currents. (b) Comparison of measured and simulated inductance.

tween the experimental and simulation results are about 6.5%, which we believe are mainly caused by the end-effects as in the stator-PM machines [23], manufacturing imperfection and measurement error.

Due to time limit, the control system of the motor is under construction and the system operation performance will be reported in the near future.

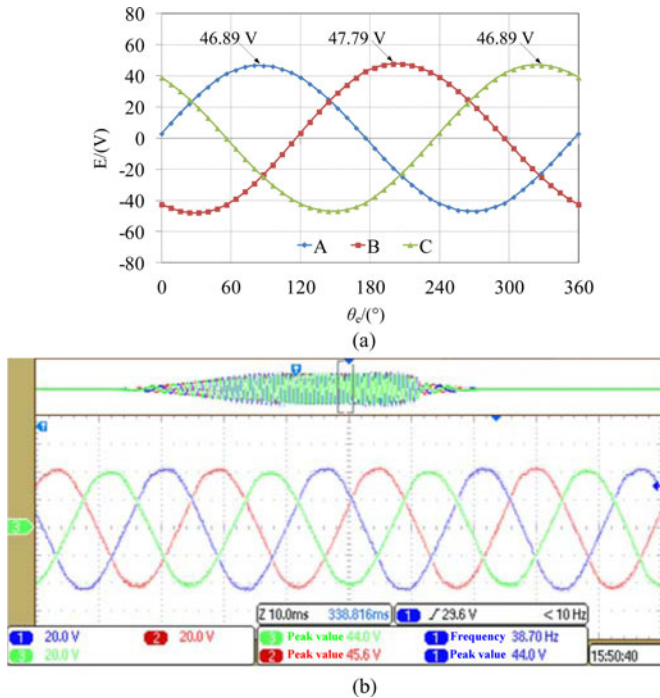


Fig. 15. Back-EMF waveforms at 1.392 m/s. (a) FEA results. (b) Experimental results.

## VI. CONCLUSION

In this paper, the structure, operation principle, and the steady-state characteristics of a new modular linear flux-switching PM motor have been analyzed. Based on the steady-state characteristics, the mathematical model of flux-linkage and self-inductance in the stator frame has been built. By using Park's transformation, the components of flux-linkage, self-inductance, voltage, and output thrust force in  $d$ - and  $q$ -axis frame have been derived. The thrust force performance based on the mathematic models is verified by FEA results. To verify the simulation results of the MLFSPM motor, a prototype motor has been built and tested. The experimental results agree well with the predicted results from the mathematic model and FEA. It, therefore, can be concluded that the mathematical model of the new MLFSPM motor has laid a foundation for future study in vector-control or thrust force-direct control for the proposed motor.

## REFERENCES

- [1] J. F. Gieras and Z. J. Piech, *Linear Synchronous Motors: Transportation and Automation Systems*. Boca Raton, FL: CRC Press, 2000.
- [2] A. Boldea and S. Nasar, *Linear Motion Electromagnetic Devices*. New York: Taylor & Francis, 2001.
- [3] T. Higuchi and S. Nonaka, "On the design of high efficiency linear induction motors for linear metro," *Electr. Eng. Jpn.*, vol. 137, no. 2, pp. 36–43, Aug. 2001.
- [4] S. Yoon, J. Hur, and D. Hyun, "A method of optimal design of single-sided linear induction motor for transit," *IEEE Trans. Magn.*, vol. 33, no. 5, pp. 4215–4217, Sep. 1997.
- [5] S. Nonaka and T. Higuchi, "Design of single-sided linear induction motors for urban transit," *IEEE Trans. Veh. Technol.*, vol. 37, no. 3, pp. 167–173, Aug. 1988.
- [6] Y. Du and N. Jin, "Research on characteristics of single-sided linear induction motors for urban transit," in *Proc. Int. Conf. Elect. Mach. Syst.*, Sep. 2009, pp. 1–4.

- [7] G. Stumberger, D. Zarko, M. T. Aydemir, and T. A. Lipo, "Design and comparison of linear synchronous motor and linear induction motor for electromagnetic aircraft launch system," in *Proc. IEEE Int. Elect. Mach. Drives Conf.*, 2003, pp. 494–500.
- [8] E. Hoang, A. H. Ben-Ahmed, and J. Lucidarme, "Switching flux permanent magnet polyphased machines," in *Proc. Eur. Conf. Power Electron.*, 1997, pp. 903–908.
- [9] Z. Q. Zhu and J. T. Chen, "Advanced flux-switching permanent magnet brushless machines," *IEEE Trans. Magn.*, vol. 46, no. 6, pp. 1447–1453, Jun. 2010.
- [10] W. Hua, M. Cheng, and Z. Q. Zhu, "Analysis and optimization of back EMF waveform of a flux-switching permanent magnet motor," *IEEE Trans. Energy Convers.*, vol. 23, no. 3, pp. 727–733, Sep. 2008.
- [11] M. Cheng, W. Hua, J. Zhang, and W. Zhao, "Overview of stator permanent magnet brushless machines," *IEEE Trans. Ind. Electron.*, vol. 58, no. 11, pp. 5087–5101, Nov. 2011.
- [12] W. Zhao, M. Cheng, W. Hua, H. Jia, and R. Cao, "Back-EMF harmonic analysis and fault-tolerant control of flux-switching permanent-magnet machine with redundancy," *IEEE Trans. Ind. Electron.*, vol. 58, no. 5, pp. 1926–1935, May 2011.
- [13] T. Raminosoa, C. Gerada, and M. Galea, "Design Considerations for a fault-tolerant flux-switching permanent-magnet machine," *IEEE Trans. Ind. Electron.*, vol. 58, no. 7, pp. 2818–2825, Jul. 2011.
- [14] M. O. E. Aboelhasan, T. Raminosoa, A. Goodman, L. D. Lillo, and C. Gerada, "A fault-tolerant control scheme for a dual flux-switching permanent magnet motor drive," in *Proc. Int. Conf. Elect. Mach. Syst.*, 2011, pp. 1–6.
- [15] Z. Q. Zhu, X. Chen, and J. Chen, "Novel linear flux switching permanent magnet machines," in *Proc. Int. Conf. Elect. Mach. Syst.*, 2008, pp. 2948–2953.
- [16] M. Jin, C. Wang, and J. Shen, "A modular permanent magnet flux-switching linear machine with fault tolerant capability," *IEEE Trans. Magn.*, vol. 45, no. 8, pp. 3179–3186, Aug. 2009.
- [17] C. Wang, J. Shen, and Y. Wang, "A new method for reduction of detent force in permanent magnet flux-switching linear motors," *IEEE Trans. Magn.*, vol. 45, no. 6, pp. 2843–2846, Jun. 2009.
- [18] R. Cao, M. Cheng, W. Hua, W. Zhao, and Y. Du, "A new primary permanent magnet linear motor for urban rail transit," in *Proc. Int. Conf. Elect. Mach. Syst.*, 2010, pp. 1528–1532.
- [19] R. Cao, M. Cheng, W. Hua, and W. Zhao, "Novel modularized flux-switching permanent magnet linear machine with complementary magnetic circuits," in *Proc. Chin. Soc. Elect. Eng.*, 2011, vol. 31, no. 6, pp. 58–65.
- [20] R. Cao, M. Cheng, C. Mi, W. Hua, and W. Zhao, "A linear doubly salient permanent magnet motor with modular and complementary structure," *IEEE Trans. Magn.*, vol. 47, no. 12, pp. 4809–4821, Dec. 2011.
- [21] R. Krishnan, *Permagnet Magnet Synchronous and Brushless DC Motor Devices*. Boca Raton, FL: CRC Press, 2010, p. 229.
- [22] S. Kim, G. Lee, J. Hong, and T. Jung, "Design process of interior PM synchronous motor for 42-V electric air-conditioner system in hybrid electric vehicle," *IEEE Trans. Magn.*, vol. 44, no. 6, pp. 1590–1593, Jun. 2008.
- [23] Z. Q. Zhu, Y. Pang, W. Hua, M. Cheng, and D. Howe, "Investigation of end effect in permanent magnet brushless machines having magnets on the stator," *J. Appl. Phys.*, vol. 99, no. 8, pp. 08R319–08R319-3, Apr. 2006.



**Ruiwu Cao** (S'10) received the B.S. degree in electrical engineering from the Yancheng Institute of Technology, Yancheng, China, in 2004, and the M.S. degree in electrical engineering from the Southeast University, Nanjing, China, in 2007, where since 2009 he has been working toward the Ph.D. degree in electrical engineering in the School of Electrical Engineering.

From 2007 to 2009, he was a Hardware Electrical Engineer with Electronic Drive System R&D center of BSH electrical Appliances (Jiangsu) CO., Ltd.

From August 2010 to November 2011, he was a joint Ph.D. student founded by China Scholarship Council with the College of Electrical and Computer Science, University of Michigan, Dearborn, where he focused on permanent magnet motors for electric vehicles, hybrid electric vehicles, and plug-in hybrid electric vehicles application. His research interests include design, analysis, and control of permanent-magnet machines.

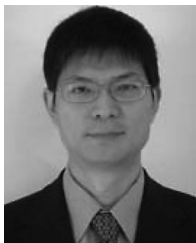




**Ming Cheng** (M'01–SM'02) received the B.Sc. and M.Sc. degrees in the Department of Electrical Engineering, Southeast University, Nanjing, China, in 1982 and 1987, respectively, and the Ph.D. degree in the Department of Electrical and Electronic Engineering, The University of Hong Kong, Pokfulam, Hong Kong, in 2001.

Since 1987, he has been with Southeast University, where he is currently a Professor in the School of Electrical Engineering and the Director of the Research Center for Wind Power Generation. From January to April 2011, he was with the Wisconsin Electric Machines and Power Electronics Consortia, The University of Wisconsin, Madison as a Visiting Professor. His teaching and research interest include electrical machines, motor drives for electric vehicles, and renewable energy generation. He has authored or coauthored more than 250 technical papers and four books, and holds 45 patents in these areas.

Dr. Cheng is a Fellow of The Institution of Engineering and Technology. He has served as the Chair and organizing committee member for many international conferences.



**Chris Mi** (S'00–A'01–M'01–SM'03–F'12) received the B.S. and M.S. degrees from Northwestern Polytechnical University, Xi'an, China, and the Ph.D. degree from the University of Toronto, Toronto, ON, Canada, all in electrical engineering.

He is an Associate Professor with the University of Michigan, Dearborn, where he is also the Director of the newly established DOE GATE Center for Electric Drive Transportation. Previously, he was an Electrical Engineer with General Electric Canada, Inc. His research interests include electric drives, power electronics, electric machines, renewable energy systems, electrical, and hybrid

vehicles. He has conducted extensive research and published more than 100 articles.

Dr. Mi is the recipient of "Distinguished Teaching Award" and "Distinguished Research Award" of the University of Michigan Dearborn. He is also a recipient of the 2007 IEEE Region 4 "Outstanding Engineer Award," "IEEE Southeastern Michigan Section Outstanding Professional Award" and the "SAE Environmental Excellence in Transportation Award." He was the Chair from 2008 to 2009) and the Vice-Chair from 2006 to 2007 of the IEEE Southeastern Michigan Section. He was the General Chair of the 5th IEEE Vehicle Power and Propulsion Conference held in Dearborn, MI, in September 6–11, 2009. He is an Associate Editor of IEEE Transactions on Vehicular Technology and IEEE Transactions on Power Electronics—Letters, a Senior Editor of the IEEE Vehicular Technology Magazine, Guest Editor of the *International Journal of Power Electronics*, Editorial Board of the *International Journal of Electric and Hybrid Vehicles*, Editorial Board of *IET Electrical Systems in Transportation*, an Associate Editor of the *Journal of Circuits, Systems, and Computers* from 2007 to 2009), and an Associate Editor for IEEE TRANSACTIONS ON INDUSTRY APPLICATION.



**Wei Hua** (M'07) was born in Jiangsu, China, in 1978. He received the B.S. and Ph.D. degrees in electrical engineering from Southeast University, Nanjing, China, in 2001 and 2007, respectively.

He is currently with Southeast University, where he is an Associate Professor and the Deputy Dean in the Department of Electrical Machines and Control. His research interests include design, analysis, and control of the novel permanent magnet machines and switched reluctance machines. He has authored more than 100 published papers on those topics.



**Xin Wang** received the B.S. degree in electrical engineering from the Hefei University of Technology, Hefei, China, in 2010. He is currently working toward the M.S. degree in the School of Electrical Engineering, Southeast University, Nanjing, China.

His research interests include control of permanent-magnet machines.



**Wenxiang Zhao** (M'08) was born in Jilin, China, in 1976. He received the B.Sc. and M.Sc. degrees in electrical engineering from Jiangsu University, Zhenjiang, China, in 1999 and 2003, respectively, and the Ph.D. degree in electrical engineering at Southeast University, Nanjing, China, in 2010.

Since 2003, he has been with Jiangsu University, where he is currently an Associate Professor in the School of Electrical and Information Engineering. His research interests include electric machine design, modeling, fault analysis, and intelligent

control.